PCCP

PAPER

View Article Online
View Journal | View Issue

Cite this: *Phys. Chem. Chem. Phys.*, 2024, **26**, 8106

Theoretical investigation of multi-spin excited states of anthracene radical-linked π-conjugated spin systems by computational chemistry†

Ken Kato *[a] and Yoshio Teki *[bc]

Received 30th December 2023,
Accepted 12th February 2024

DOI: 10.1039/d3cp06335f

rsc.li/pccp

Multi-spin excited states of chromophore radical-linked π-conjugated spin systems are investigated by molecular orbital calculations based on density functional theory (DFT). The investigated systems consist of an anthracene photosensitive unit leading to a triplet-excited-state (S = 1), π-conjugated linker to propagate spin exchange-coupling, and stable organic radical with a doublet-ground-state (S = 1/2). The intramolecular exchange coupling (J_{DQ}), g value, and fine-structure interaction of their excited states depended on the π-conjugation network (π-topology), type of radical, and molecular structure of the π-linker (length and dihedral angle). The exchange interaction was dependent on the π-topology and the type of radical species. A decrease in the dihedral angle between the anthracene moiety and phenyl linker in the photo-excited state led to larger exchange coupling. With an increase in the π-linker length (r), the magnitude of the exchange coupling gradually decreased in the photoexcited states according to $J_{DQ} = J_0^{Ex}\exp(-\beta r)$, similar to the ground-state exchange. The g values of the quartet (Q) state depended only on the radical type (independent of the linker). Conversely, the fine-structure interaction of the Q state was independent of the radical type and depended on both the linker length and the dihedral angle.

Introduction

Multi-spin excited states of photoexcited chromophore-radical linked systems are of current interest in chemistry and materials science.[1–3] Strong exchange coupling between the excited-triplet-state (S = 1) of the chromophore and doublet-state (S = 1/2) of the radical substituent achieves a robust spin alignment, acting as an optical switch in the molecular spin state.[1] On the other hand, the weak exchange interaction between them leads to electron spin hyperpolarisation by a variety of mechanisms[4–7] such as radical–triplet pair mechanisms (RTPMs), electron spin polarization transfer (ESPT) or reverse quartet mechanisms (RQM). These polarization transfer mechanisms involve not only exchange interactions but also magnetic parameters such as fine-structure interactions and g values.[8–12] The exchange interaction also causes enhancement/acceleration of the intersystem crossing (EISC) of the chromophore. EISC is suggested by three possible mechanisms:[1] electron spin exchange (strictly speaking, exchange integral) between a SOMO on the radical and the HOMO or LUMO on the singlet excited chromophore (this mechanism is usual EISC),[13,14] spin–orbit interaction borrowing the radical moiety,[15] and ISC *via* higher-energy state.[16,17] Several applications of EISC have been reported, such as preventing the decomposition of light-unstable materials[18–20] and upconversion by triplet–triplet annihilation[21] and information transfer.[22,23] Understanding the dependence of molecular structure (*e.g.*, type of radical substituent, π-topology and linker length) on the exchange interaction and magnetic parameters is important to exploit the photoexcited chromophore-radical linked systems in molecular-based future technology such as molecular spintronics devices or information science applications.

We have reported high-spin photoexcited states of anthracene radical-linked π-conjugated spin systems and demonstrated the control of the spin states utilizing their π-topology.[15,24–27] The energy relaxation process with spin conversion in the multi-spin excited states and the schematic picture of electron configuration in each state are shown in Fig. 1. The energy gap between the lowest quartet photo-excited state (Q) and the lowest doublet photo-excited state (D) depends on the magnitude of the exchange coupling constant (J_{DQ}) between the triplet-state (S = 1) of the excited chromophere and the doublet-state (S = 1/2) of the radical substituent, and the order of the energy level changes according to the sign of J_{DQ}. Several studies to clarify the magnitude and sign of J_{DQ}

[a] *Institute for Protein Research, Osaka University, 3-2 Yamadaoka, Suita-shi, Osaka 565-0871, Japan. E-mail: katoken@protein.osaka-u.ac.jp*
[b] *Graduate School of Science, Osaka City University, 3-3-138 Sugimoto, Sumiyoshi-ku, Osaka 558-8585, Japan*
[c] *Graduate School of Engineering, Osaka Metropolitan University, 3-3-138 Sugimoto, Sumiyoshi-ku, Osaka 558-8585, Japan. E-mail: teki@omu.osaka-cu.ac.jp*

† Electronic supplementary information (ESI) available. See DOI: https://doi.org/10.1039/d3cp06335f

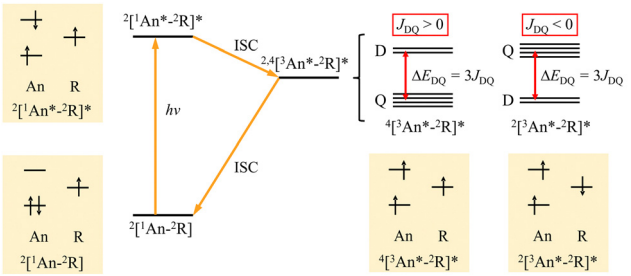

Fig. 1 Excited-state processes and schematic picture of the electron configuration of anthracene–radical linked system.

have been reported,[12,28,29] but in experiments, the magnitude of J_{DQ} that can be measured is limited. In addition, although the estimation of J_{DQ} between the triplet excited state and radical spin has been carried out using the broken symmetry density functional theory (DFT) or complete active space self-consistent field (CASSCF) methods,[30–33] there are still limited comprehensive investigations for the molecular structure of the coupling moiety (π-linker) together with structural evaluation of exchange interactions, fine-structure interaction and g values. In this paper, we report the DFT calculations of electron spin interactions in the photo-excited anthracene–radical π-conjugated systems to understand how the magnetic parameters depend on them.

Methods

All calculations were carried out using an ORCA 5.0.3 program package.[34] Molecular structure visualisation and spin density mapping were performed using Avogadro.[35] The D state (pseudo-doublet excited state) used for the estimation of J_{DQ} was calculated for the optimized geometry of the Q state by the broken-symmetry DFT. The J_{DQ} between the triplet excited state of the anthracene moiety (^{3}An*) and doublet radical moiety (^{2}R) was expressed using the Heisenberg–Dirac–van Vleck (HDvV) spin Hamiltonian,

$$\hat{\boldsymbol{H}}_{HDvV} = -2J_{DQ}\boldsymbol{S}_T\cdot\boldsymbol{S}_R \quad (1)$$

where $\boldsymbol{S}_T$ and $\boldsymbol{S}_R$ are the spin operators of the triplet excited state of the anthracene moiety (chromophore) and the doublet state of the radical substituent, respectively. In this notation, a negative J value corresponds to an antiferromagnetic interaction, whereas a positive one is related to a ferromagnetic interaction. Since the D state obtained by the broken-symmetry DFT calculation has spin contamination from higher-energy spin states, the calculated energy is overestimated. For the Hamiltonian (1), J_{DQ} can be related to the energy difference (ΔE_{DQ}) between D and Q as $J_{DQ} = 3\Delta E_{DQ}$ when the spin contamination is negligible. In the DFT calculations, an approximate spin projection is used to remove the effect of spin contamination. Thus, J_{DQ} can be estimated by Yamaguchi equation (eqn (2)),[36]

$$J_{DQ} = \frac{E_{BS} - E_{HS}}{\langle S^2\rangle_{HS} - \langle S^2\rangle_{BS}} \quad (2)$$

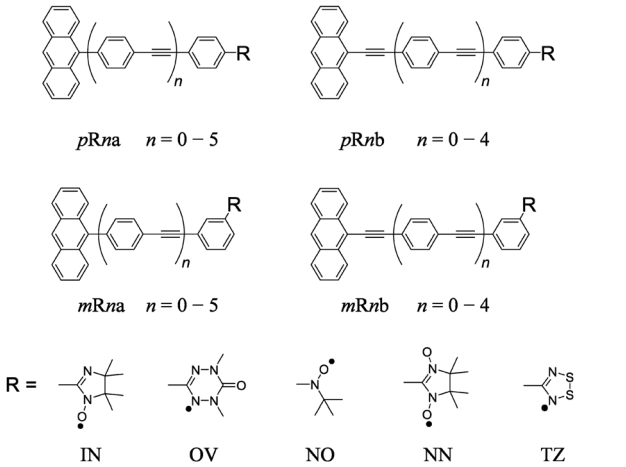

Fig. 2 Molecular structure of anthracene π-conjugated stable radical used in this work.

where $\langle S^2\rangle_{HS}$ and $\langle S^2\rangle_{BS}$ are the expected values of S^2 for the high spin (HS) and broken symmetry (BS) states obtained in the DFT calculations, respectively.

In this work, we have treated a series of anthracene coupled to stable radicals with π-conjugated linker (π-linker) shown in Fig. 2. Here, two types of π-topology are connected to the anthracene excited chromophore at *meta* (*m*) or *para* (*p*) position of the phenyl group in the linker by the radical moiety. Five kinds of radical substituents (**IN**: imino nitroxide, **OV**: 1,5-dimethyl-6-oxoverdazyl, **NO**: *tert*-butyl nitroxide, **NN**: nitronyl nitroxide, and **TZ**: 1,2,3,5-dithiadiazolyl) and a series of oligo-phenylene ethynylene linkers with different lengths (*n* means the number of phenyl-ethynyl repeating units) are investigated. We denote their molecules as ***p*(*m*)Rn**a(b), where *p*(*m*), R, *n* and a(b) mean the type of π-topology, kind of radical species, number of phenyl-ethynyl repeating units in the π-linkers, and type of π-linker, respectively.

Geometry optimizations of doublet ground state (D_0) and Q state were performed by DFT using unrestricted-B3LYP/6-31G(d,p) basis sets. The fine-structure interaction and $\boldsymbol{g}$ tensors of Q state and D state using broken symmetry DFT were calculated for the optimized geometry. The spin–spin term ($\boldsymbol{D}_{SS}$) of the fine-structure tensor was estimated using the unrestricted natural orbital (UNO). A full table of the results of the calculations is shown in the ESI.†

Results and discussion

The functional and basis-set dependencies were checked for ***p*OV0a**. In ***p*OV0a**, the sign and magnitude of J_{DQ} (broken-symmetry method), g value, and zero-field splitting parameters (D and E) were almost independent of each functional, such as B3LYP, CAM-B3LYP, B3PW91 and O3LYP, and basis sets such as 6-31G(d,p), 6-311G(2d,2p), def2-SVP and def2-TZVP (Table S1, ESI†). The calculated J_{DQ} values by the CASSCF method became smaller than those by the broken-symmetry method according to the increase in the active space and by adding

perturbations. However, the magnitudes were still in the same order. It is reported that the calculated J_{DQ} values of minimal CASSCF with multi-reference perturbation theory methods underestimate the exchange interactions by 60–80%.[33] For organic diradicals in the ground state, the exchange interaction (J) is known to be overestimated by DFT methods that include large amounts of Hartree–Fock exact exchange, such as the B3LYP method, but agrees to some extent with experimental values by the application of appropriate scaling factors.[37] When the writing of this paper was completed, a preliminarily experimental result for ***p*OV1a** was obtained, which suggested probably a fairly smaller J value than that of CASSCF.[38] This may be a problem peculiar to multi-spin systems. However, there are still many unanswered issues, such as the cause of the issue, generality, solvent matrix effects and so forth. Therefore, in this work, the calculation and discussions will proceed using the traditional and widely used calculation methods. Although the absolute value of the exchange interaction may be inaccurate, the discussion focuses on the trend for the π-linker structure, which is more reliable. The broken-symmetry method using B3LYP/6-31G(d,p) is a popular method with low computational cost. Therefore, in this work, we chose this method to clarify the trend of J_{DQ} in terms of molecular structure in further discussions.

It is well established both experimentally and theoretically that the spin polarization effect plays an important role in the spin alignment in the ground state and the photo-excited state of π-conjugated spin systems.[1,3,15,39] Fig. 3a shows that the spin alignment is qualitatively understood by taking the spin polarization effect depicted by the arrows into account (the arrow direction indicates the sign of the spin density and the alternating sign of the spin density between the adjacent carbon atoms is expected from the spin polarization effect). The lowest excited states were detected by the time-resolved ESR measurements,[40] but it was difficult experimentally to detect higher energy spin states with different spin multiplicities, except when they were in energy proximity.[41–43] Theoretical calculations can approach the electronic states that are not accessible experimentally, and therefore, making it possible to estimate the intra-molecular exchange interaction in the π-conjugated multi-spin photoexcited systems.

Fig. 3b and c show the calculated total energy and spin densities of ***p*IN0a** and ***m*IN0a**, respectively. The lowest excited states of ***p*IN0a** and ***m*IN0a** were Q and D states, respectively, which agreed with the results of the TRESR experiments.[15] In the lowest excited states of ***p*IN0a** and ***m*IN0a**, the spin density distribution in the phenyl group jointing the triplet anthracene to the radical moiety is consistent with the qualitative picture in Fig. 3a. The J_{DQ} of ***p*OV0a** calculated from eqn (2) was close to the experimental result[29] and the previous theoretical calculation.[30,31] The dihedral angles (ϕ) between the anthracene moiety and the adjacent phenyl group were 73.1° and 58.6° in the ground and excited states of ***p*IN0a**, respectively. These values were also close to those of the previous theoretical studies.[30,31]

Radical species and π-topology dependencies of exchange interactions and dihedral angles

Since the rate of intersystem crossing (ISC) depends on the potential energy surfaces between the initial and final states, the molecular structure in the excited state is an important factor related to the rate.[44,45] Here, we selected the subtraction of the dihedral angle between the ground and excited states ($\Delta\phi$) as the index of the spin (unpaired electron) delocalization in the photo-excited states, which are characteristics in the photo-excited states with singly occupied ''HOMO'' and ''LUMO''. We compared the exchange interaction between the radical moiety and the chromophore to their $\Delta\phi$ in the excited state. Fig. 4 shows the radical species dependencies of the J_{DQ} value and $\Delta\phi$ of ***p*(*m*)R0a**. The dihedral angle (ϕ) between the anthracene and phenyl moieties depicted in Fig. 5a is indicated on the right axis of Fig. 4. The ***p*(*m*)IN0a**, ***p*(*m*)OV0a**, ***p*(*m*)NN0a**, and ***p*(*m*)TZ0a** gave ferromagnetic interactions in the *para*-joint type (p) and antiferromagnetic interactions in the *meta*-joint type (m). Only ***p*(*m*)NO0a** showed the opposite trend: antiferromagnetic in the *para*-joint type (p) and ferromagnetic in the *meta*-joint type (m). This result is due to the direct bonding of the **NO** group with large spin density to the π-linker.[27] On the other hand, the radical species dependence in the magnitude of

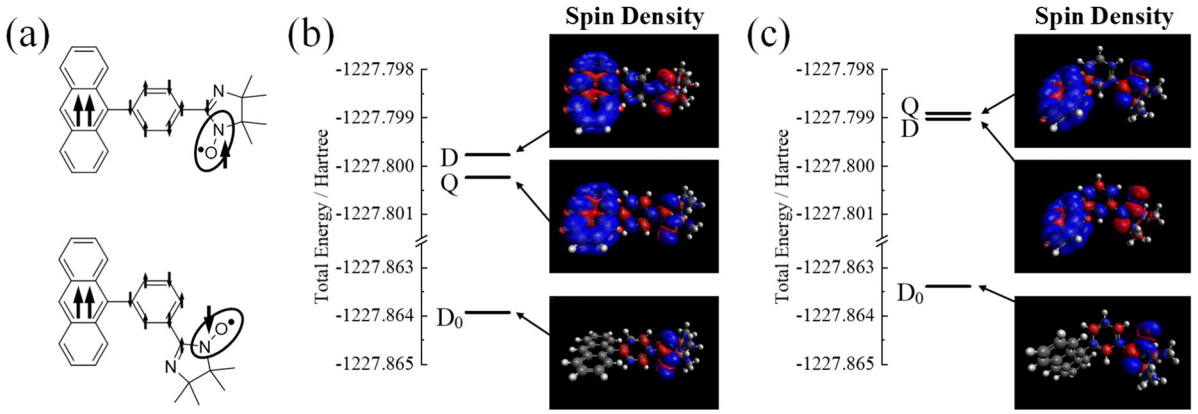

Fig. 3 Spin alignment and photo-excited states of ***p*IN0a** and ***m*IN0a**. (a) Schematic picture of the spin alignment in the lowest photo-excited state of ***p*IN0a** and ***m*IN0a**. (b) Total energy and spin density mapping of ***p*IN0a**. (c) Total energy and spin density mapping of ***m*IN0a**.

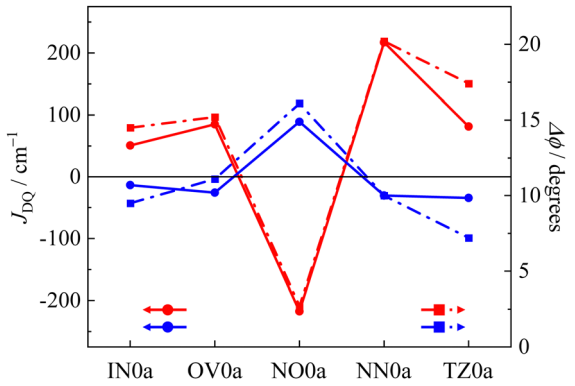

Fig. 4 J_{DQ} *vs.* $\Delta\phi$ plot. Closed circles and closed squares are J_{DQ} values and $\Delta\phi$ values, respectively (red: *para* joint, blue: *meta* joint).

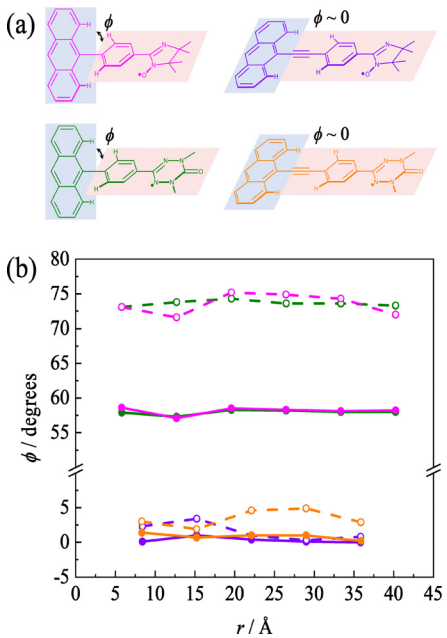

Fig. 5 (a) Molecular structure of ***p*IN0a** (pink), ***p*OV0a** (green), ***p*IN0b** (orange) and ***p*OV0b** (violet). (b) Dihedral angles (ϕ) in a series of ***p*IN*n*a** (pink), ***p*OV*n*a** (green), ***p*IN*n*b** (orange) and ***p*OV*n*b** (violet) with the different length oligophenylene ethynylene linkers; ground state (open circle) and excited state (closed circle).

J_{DQ} is regardless of their π-topology; that is, $|J_{DQ}|$ is larger in the *para*-joint type than in the *meta*-joint type. The magnitude of the effective exchange interaction in the ground state of the π-conjugated multi-spin systems is proportional to the spin densities (ρ_i^A and ρ_j^B) between the connecting sites i and j, when the two moieties (A and B) are weakly interacting (corresponding to the disjoint case in the category of Borden and Davidson[46]), that is, $J^{eff} = J_{ij}\rho_i^A\rho_j^B/4S^AS^B$.[39,47,48] Thus, if the phenyl group is regarded as a spin-coupler, the *meta* position has a small spin density, resulting in a small exchange interaction. A similar trend was observed in the J_{DQ} values of the excited states.

All ***p*R0a** series has a twisted conformation of the phenyl linker about $\phi \sim 75^\circ$ for the anthracene chromophore in the ground state due to the steric hindrance between the anthracene moiety and the attached phenyl group, which is independent of radical substituents and π-topology. In the previous theoretical studies for ***p*OV0a** and ***p*IN0a**, the ϕ in the Q state is reported to be $\sim 56^\circ$,[30] which is much flatter than that of the ground state and also smaller than 67° of the T_1 state of phenyl-anthracene (the details as shown Fig. S1, ESI†). In the present calculations, the structural optimization of the Q state in the *para*-joint type, except for the *tert*-butyl nitroxide radical (**NO**) species, gave almost the same tendency as in the previous report.[30,31] Thus, attachment of the radical substituents leads to a decrease of ϕ in the Q states compared to the T_1 state of phenyl-anthracene. The ϕ in the Q states of ***p*NN0a** and ***p*TZ0a** was much flatter than that of the D_0 state. The decrease in ϕ leads to more propagation through π-conjugation, in which the magnetic interaction becomes larger. Thus, a decreasing ϕ in the excited state leads to increasing $|J_{DQ}|$. Therefore, the ***p*NN0a** with the largest exchange interaction in the *para* joint type also has the largest change in dihedral angle, that is, the largest $\Delta\phi$. In contrast, the optimized structures of the Q state in the *meta*-joint type, except the *tert*-butyl nitroxide radical (**NO**) species, gave almost the same dihedral angle as that of the T_1 state of the phenyl-anthracene, which indicates a small amount of electronic and magnetic stabilization between the anthracene and phenyl moiety. For **NO0a** with a large spin density directly bonded to the π-linker, the signs of J_{DQ} and $\Delta\phi$ in the Q state are opposite to those of other radical species. These calculations show that in all molecules calculated here, the subtraction of the dihedral angle ($\Delta\phi$) between the ground and excited states correlates well with the J_{DQ} values. These findings mean that in the **a** type molecules, $\Delta\phi$ works as an excellent index of the excess spin (unpaired electron) delocalization characteristics in the photo-excited states.

Linker dependence of exchange interactions and dihedral angles

Since the dihedral angle increases by the steric hindrance between the anthracene moiety and the attached phenyl group, the insertion of an ethynyl group between them decreases the steric hindrance significantly, as shown in Fig. 5a. Thus, the **b** type molecules have smaller dihedral angle than the **a** type molecules. The changes in the structure and the magnetic parameters were calculated for both types when the number of phenyl–ethynyl repeating units, that is, the linker length, was varied in the π-linker. The dihedral angles (ϕ) between the anthracene moiety and the phenyl group *vs.* linker length plot is shown in Fig. 5b. Here, the linker length (r) was defined as the distance between the carbon atoms at the 9-position of anthracene and the carbon atoms of **OV** or **IN** at the joint position to the π-linker. Similar to the previous section, the ϕs in the excited state and ground state for the ***p*IN*n*a** and ***p*OV*n*a** series (n: the number of phenyl–ethynyl repeating units) were around 57° and 73°, respectively, independent of the linker length. In contrast, the ϕs for the ***p*IN*n*b** and ***p*OV*n*b** series were close to zero in both the excited and ground states, leading to

$\Delta\phi \sim 0$. This trend was also observed for other radical species and *meta*-joint molecules.

There is no systematic study of the exchange interaction in the π-conjugated multi-spin organic systems in the photo-excited state. Therefore, although the exchange interactions between excited triplet-state chromophores and stable radicals may have similar characteristics to those of the ground state spin systems, it is worth examining the behaviour. In the ground-state biradical systems, the exchange interaction through π-conjugation between radical substituents was studied experimentally and computationally.[49–54] In this ground-state biradical system, the exchange interaction is reported to decay exponentially as follows:[49]

$$J = J_0 \exp(-\beta r) \quad (3)$$

where β and r were the decay constant and the linker length, respectively. The exchange interaction can be determined experimentally by analysing the shape of the ESR spectra when the magnitude of the exchange interaction is comparable to the hyperfine coupling constant.[50,51] It was also estimated by the broken symmetry DFT calculations. In these results, the decay constant due to π-bonding was independent of the type of radical substituent and varied significantly with the structure of the linker.[52–55] In addition, the conductance of a single molecular π-conjugated wire decreased exponentially with increasing number of the repeating units of the π-linker.[56–58] The linker species dependence of the decay constant β of the conductance was in good agreement with that of the exchange interaction in the case of the neutral radicals. The exchange interaction between charge-separated radical pairs *via* oligophenylene groups was also investigated using magnetic field effects on triplet yields of photoinduced electron transfer reactions.[59] The distance dependence of the rate constant in the charge separation and the recombination processes was also exponential decay, and their decay constants (β) were consistent with those of the exchange interaction between photoinduced radical pairs.[60–62] In this work, we investigated the decay of the exchange interaction in the multi-spin photo-excited systems for the repetition number of the phenyl–ethynyl group in the π-linker, which connects the anthracene triplet-state chromophore to the radical substituents. A plot of $\ln|J_{DQ}|$ *vs.* the linker length is shown in Fig. 6. Since in some molecules of the **IN*n*b** series, the broken symmetry DFT calculation converged to the D_0 state, not the D state, they are not shown in Fig. 6. The slope in the plot of $\ln|J_{DQ}|$ to the linker length corresponds to the decay constant, β. The β values of ***p*OV*n*a**, ***p*OV*n*b**, and ***p*IN*n*b** series were determined to be 0.239, 0.241 and 0.239 $Å^{-1}$, respectively. The β values in the equation, $J_{DQ} = J_0^{Ex}\exp(-\beta r)$, determined in this study, showed similar characteristics to the ground-state bi-radicals, that is, independent of the type of the radical species and the π-topology (see Fig S2–S6 and Table S4, ESI†). Here, J_0^{Ex} corresponds to J_0 values on the multi-spin photoexcited states. These β values in the photo-excited states were close to the reported ones of exchange interactions between neutral bi-radicals (β = 0.24 $Å^{-1}$) and the single molecular conductance (β = 0.27 $Å^{-1}$) of the oligophenyl-ethynyl linker. This result indicates that the β value through the π-linker is independent of whether the excited state or ground state and their spin quantum numbers.

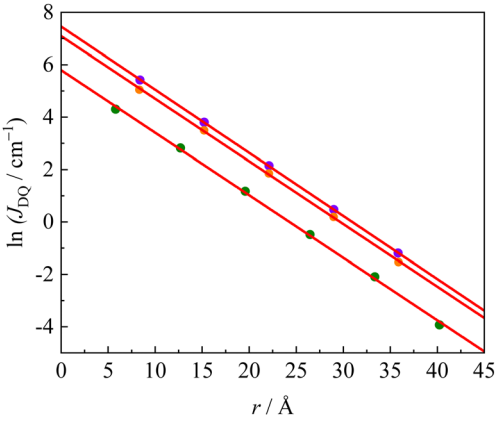

Fig. 6 Linker length dependence on J_{DQ}; ***p*IN*n*b** (orange), ***p*OV*n*a** (green) and ***p*OV*n*b** (violet) series. The red lines are linear fittings using eqn (3).

On the other hand, J_0^{Ex} depended on the radical species, π-topology and linker structure. The dependence is already explained in the previous section. The J_0^{Ex} values of oxo-verdazyl radical series, ***p*OV*n*a**, ***p*OV*n*b**, ***m*OV*n*a**, and ***m*OV*n*b** were 329, 1737, −144 and −593 cm^{-1}, respectively. Although ***p*OV0b** and ***m*OV0b** have a π-linker longer than those of ***p*OV0a** and ***m*OV0a**, they show larger J_{DQ} values. In the case of the direct orbital-conjugation, the propagation of the exchange interaction *via* the π-linker is expected to be related to the overlap integral of the two molecular-atomic orbitals (probably natural orbitals) at the joint position between the linker and triplet chromophore. Therefore, intramolecular exchange interaction depends on the dihedral angle (ϕ), as follows:[63–65]

$$J_0^{EX} \propto \cos^2\phi \quad (4)$$

As shown in Fig. 7, the overlap integral of the phenyl anthracene unit is expected to be smaller than that of the phenylethynyl anthracene unit because of the larger dihedral angle. ***p*(*m*)OV*n*a** shows $\cos^2\phi$ = 0.28 because of the large dihedral angle (ϕ = 57.9°) of the Q state. In contrast, in ***p*(*m*)OV*n*b**, shows $\cos^2\phi \sim 1$ because of the small dihedral angle (ϕ = 0.1°). Matsuda *et al.* reported almost the same β as ours, and the linker length dependence was also a similar exponential decay (eqn (3)). When J_0 was calculated backward according to eqn (3) using their data, $J_0 \sim -370$ cm^{-1}.[52] This magnitude is of the same order as J_0^{EX} of ***p*OV*n*a**. Since the unpaired electron in the SOMO of the radical moiety interacts with both the unpaired electrons in the HOMO and the LUMO of the chromophore in

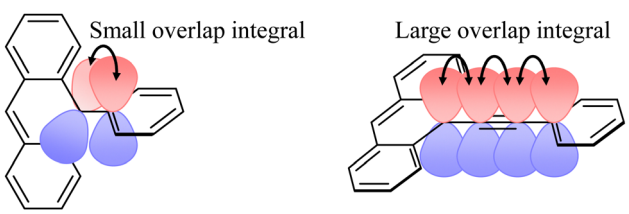

Fig. 7 Schematic view of π-orbital overlap in phenyl anthracene (left) and phenylethynyl anthracene (right).

the excited state, J_0^{EX} is expected to become larger than J_0 of the ground-state biradical systems, but the smaller value for ***p*OV*n*a** is probably due to the larger dihedral angle.

ESR parameters of Q state on the anthracene π-conjugated stable radical systems

When the molecule has a spin quantum number of $S \geq 1$, the ESR spectrum shows zero-field splitting due to the magnetic interactions between unpaired electrons. They are characterized by the effective spin Hamiltonian given by

$$\hat{\boldsymbol{H}} = \mu_B \boldsymbol{B}\cdot\boldsymbol{g}\cdot\boldsymbol{S} + \boldsymbol{S}\cdot\boldsymbol{D}\cdot\boldsymbol{S} \quad (5)$$

where μ_B, $\boldsymbol{g}$, and $\boldsymbol{D}$ are Bohr magneton, the electron g tensor, and fine-structure tensor, respectively. Although the higher order term in $\boldsymbol{S}$ is a group theoretically allowed in the fine-structure term, they are negligible in the molecules constructed from only light atoms. The $\boldsymbol{g}$ and $\boldsymbol{D}$ are important factors that determine not only the shape of the ESR spectrum but also the behaviour of the polarization transfer and the magnetic field effects in the excited states. In the anthracene – radical π-conjugated spin systems, the anisotropy of the $\boldsymbol{g}$ tensor is sufficiently small compared to the zero-field splitting. Here, we treated the systems as an isotropic g value, which is the averaged value, $(g_{xx} + g_{yy} + g_{zz})/3$. The fine structure tensor can be characterized in terms of the zero-field splitting parameters (D and E). The spin sublevels of the spin systems with $S \geq 1$ are, therefore, resolved by the fine-structure term even without the external magnetic field, known as zero-field splitting.

When the quartet state is constructed from the radical–triplet pair, the $\boldsymbol{g}$ tensor is given by the following equation:[66]

$$\boldsymbol{g}(Q) = \frac{2}{3}\boldsymbol{g}(T) + \frac{1}{3}\boldsymbol{g}(R) \quad (6)$$

A comparison of the g values obtained by the DFT calculation and by eqn (6) is shown in Fig. 8. The g values for the triplet-state of anthracene and each radical are summarized in Table S7 (ESI†). The results of the g value calculations using DFT and eqn (6) were in good agreement with the experimental results.

However, the estimations using eqn (6) were slightly better than the g values calculated directly using the DFT calculation of the whole molecule. In this DFT calculation, the following multiple terms contribute to the $\boldsymbol{g}$ tensor.

$$\boldsymbol{g} = g_e\boldsymbol{1} + \Delta\boldsymbol{g}_{RMC} + \Delta\boldsymbol{g}_{DSO} + \Delta\boldsymbol{g}_{PSO} \quad (7)$$

where g_e, $\Delta\boldsymbol{g}_{RMC}$, $\Delta\boldsymbol{g}_{DSO}$ and $\Delta\boldsymbol{g}_{PSO}$ are the isolated electron's g factor, relativistic mass correction, diamagnetic spin–orbit term, and paramagnetic spin–orbit term, respectively. In general, the largest contribution to the shift from g_e (free electron g value; 2.0023) is the $\Delta\boldsymbol{g}_{PSO}$ term. The large g value shift of the **TZ** radical can be explained by the sulphur atom, in which the spin–orbit interaction is larger than that of the other constructed elements, resulting in a larger $\Delta\boldsymbol{g}_{PSO}$ in the g value. The linker dependence of the calculated g value of the Q state is shown in Fig. 9. The g values of the ***p*(*m*)OV*n*a** series are similar to those of the ***p*(*m*)OV*n*b** series. The same finding holds between ***p*(*m*)IN*n*a** and ***p*(*m*)IN*n*b** series. Thus, the g values are independent of the linker structure (length and dihedral angle) and only dependent on the radical species. This means that the effect of the spin delocalization on the linker is negligible in the g value, even in the type **b** structures. In such cases, the g value is explained by eqn (6), in which $\boldsymbol{g}$(Q) depends only on $\boldsymbol{g}$(R) because $\boldsymbol{g}$(T) is dominantly determined by the triplet state of the anthracene chromophore.

The fine-structure tensor consists of $\boldsymbol{D}_{SS}$ and $\boldsymbol{D}_{SO}$ terms that are due to magnetic dipole–dipole interactions (spin–spin interactions) and spin–orbit coupling, respectively. The contribution of the $\boldsymbol{D}_{SO}$ term is small in organic materials composed only of light elements such as H, C, N and O because the spin–orbit coupling is proportional to the fourth power of the atomic number of the constituent elements. The pq matrix-element in the $\boldsymbol{D}_{SS}$ tensor term is given by

$$D_{pq} = \frac{\mu_0}{4\pi}\frac{1}{2S(S-1)}\left\langle\psi\left|\frac{\delta_{pq}r_{ik}^2 - 3p_{ij}q_{ij}}{r_{ik}^5} \times \left(2s_{iz}s_{jz} - s_{ix}s_{jx} - s_{iy}s_{iy}\right)\right|\psi\right\rangle \quad (8)$$

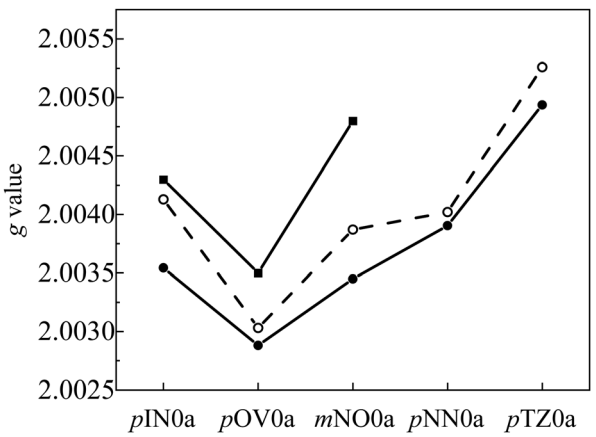

Fig. 8 Calculated g values of the Q states of the anthracene–radical π-conjugated spin systems; DFT method (closed circle), eqn (6) (open circle) and experimental (closed cube).

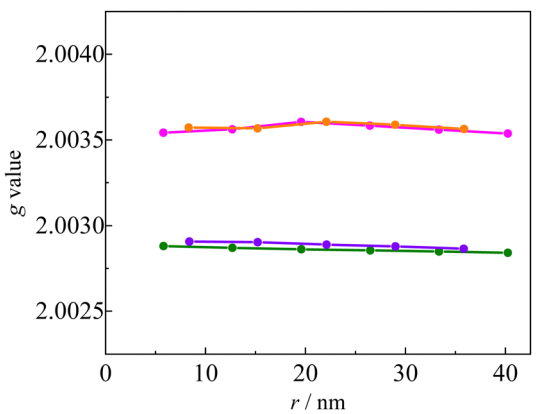

Fig. 9 Calculated g values of the Q states of ***p*IN*n*a** (pink), ***p*OV*n*a** (green), ***p*IN*n*b** (orange), and ***p*OV*n*b** (violet)

When the wavefunction is approximated by a single electron configuration, it can be obtained from the spin density matrix.[67]

$$D_{pq} = \frac{\mu_0}{4\pi}\frac{1}{2S(S-1)}\sum_{\mu\nu}\sum_{\kappa\tau}\left(P^{\alpha-\beta}_{\mu\nu}P^{\alpha-\beta}_{\kappa\tau} - P^{\alpha-\beta}_{\mu\kappa}P^{\alpha-\beta}_{\nu\tau}\right) \times \left\langle \mu\nu\left|\frac{\delta_{pq}r_{ik}^2 - 3p_{ij}q_{ij}}{r_{ik}^5}\right|\kappa\tau\right\rangle \quad (9)$$

Here, $P^{\alpha-\beta}$ is the spin density matrix obtained by the DFT calculation. It is known that, in the estimation of the $\boldsymbol{D}_{SS}$ term, the wavefunction obtained by the restricted open-shell method (RODFT) gives better results than the unrestricted method (UDFT).[68] The unrestricted natural local orbital (UNO) calculated by the diagonalization of the density matrix obtained from the wave function have been reported to give better agreement than the DIRECT method in UDFT.[68] It is reported that the calculated $\boldsymbol{D}_{SS}$ term by the UNO method were close to that of the RODFT.[69] The RODFT method has poor convergence in SCF calculations; in this work, we chose the UNO method. It is also known that the $\boldsymbol{D}_{SS}$ term obtained by the DFT calculation is underestimated when the unpaired electrons are distributed in the same π electron framework, such as the ππ* excited states of aromatic hydrocarbons.[69] When the quartet state is constructed from the radical–triplet pair, the $\boldsymbol{D}$ tensor of the Q state is given by the following:[66]

$$\boldsymbol{D}(\mathrm{Q}) = \frac{1}{3}\boldsymbol{D}(\mathrm{T}) + \frac{1}{3}\boldsymbol{D}(\mathrm{RT}) \quad (10)$$

$\boldsymbol{D}$(T) and $\boldsymbol{D}$(RT) are the fine-structure tensors for the triplet excited state and the magnetic dipolar–dipolar interaction between the radical and the triplet moieties. We denote that D(T) and D(RT) correspond to the contributions from $\boldsymbol{D}$(T) and $\boldsymbol{D}$(RT) in the zero-field splitting parameter (D), respectively. D(RT) is proportional to r^{-3} when a point dipole approximation of the triplet anthracene and the radical is used:

$$D^{\mathrm{dipole}}(\mathrm{RT}) = \frac{3\mu_0}{8\pi}\frac{(g\beta)^2}{\langle r^3\rangle} \quad (11)$$

As shown in Fig. 10a, D(Q) obtained by the DFT calculation for the ***p*INN*n*a** series agreed well with the estimated values using eqn (10), in which D(T) and D(RT) were obtained by the DFT calculation for the molecules without radical substituents and by the point dipole approximation, respectively. However, the calculated D_{SS}(Q) value (the contribution from $\boldsymbol{D}_{SS}$ term in the D value) of ***p*IN0a** was only about 60% of the experimental one because the $\boldsymbol{D}$(T) term was under-estimated by half (Fig. 10b). Although the CASSCF method using a large active space can estimate the $\boldsymbol{D}_{SS}$ tensor more accurately,[70] it is too computationally expensive for the large-size molecules as treated in this work. Therefore, although the magnitudes are underestimated, we discuss only a trend in magnetic dipole interactions of radicals *via* the π-linker to the triplet-state of the anthracene chromophore by DFT calculations. Fig. 11 shows the linker dependence of the D_{SS} value obtained by the restricted B3LYP method using 6-31G(d,p) basis sets. Similar length dependence

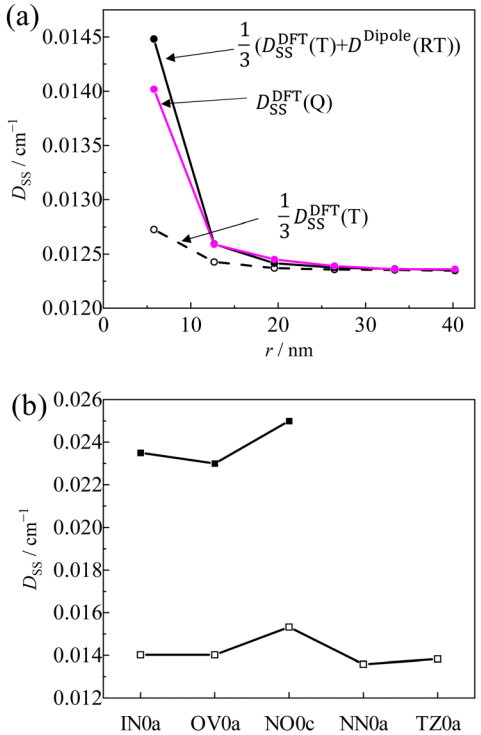

Fig. 10 (a) Linker dependence on the D value of ***p*IN*n*a** series by DFT (pink), eqn (10) (closed circle) and one third of the D value of T_1 state of without radical moiety by the DFT (open circle), (b) calculated D value (open cube) and experimental D value (closed cube) of the Q states.

was observed in $\boldsymbol{D}_{SS}$ calculations with other basis sets, such as restricted open BP/EPR-II and unrestricted CAM-B3LYP/def2-TZVP (Fig. S7, ESI†). The D values of the ***p*OV*n*a(b)** series were similar to those of ***p*IN*n*a(b)**. This behaviour is the opposite of the structure dependence of the g value, that is, the D values are independent of the radical species and only influenced by the linker structure (length and dihedral angle). For example, the D_{SS} value of ***p*OV5a** was larger than that of ***p*OV4b** despite the fact that it has a longer linker length. Thus, D_{SS} depends not only on the linker length r, but also on the dihedral angle ϕ. In the ***p*OV*n*b** and ***p*IN*n*b** series, the unpaired electrons in the

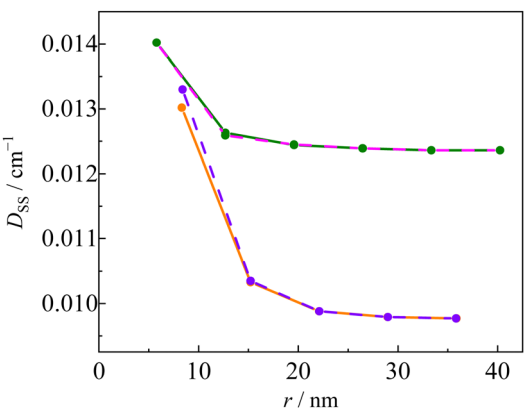

Fig. 11 Calculated D value of the Q states of **IN*n*a** (pink), **OV*n*a** (green), **IN*n*b** (orange), and **OV*n*b** (violet) series.

triplet-state of the anthracene chromophore are expected to delocalize to the linker due to the small dihedral angle ϕ between the anthracene and phenyl groups. The $\boldsymbol{D}$(T) in eqn (10) of the type **b** linker series is smaller in magnitude than that of the type **a** linker sers because the molecular orbital of the triplet chromophore is delocalized, and consequently, the D(Q) of the type **b** linker series becomes smaller.

Conclusion

The exchange interactions, g values, and fine-structure interactions in the quartet (Q) excited states of the anthracene–radical π-conjugated systems were systematically investigated by DFT calculations. Based on the results of structure optimizations for the ground and excited states and J_{DQ} calculations by the broken symmetry DFT for the excited states, the smaller $\Delta\phi$ leads to the larger exchange interaction between the triplet anthracene and the radical. The steric hindrance was removed by inserting the ethynyl group between the anthracene and phenyl groups, and the ϕ of the ground and excited states were close to zero, resulting in a large J_{DQ}. The decay constant β. of the exchange interaction *via* the π-linker between anthracene and the stable radical was almost identical to the ground state. The g values of the Q state depended only on the radical type, which was independent of the linker structure. Conversely, the fine-structure tensor of the Q state was independent of the radical type and depended on the linker length and dihedral angle.

We reported that, in the triplet chromophore–radical linked systems, the enhanced intersystem crossing led to significant photo-chemical stabilization for pure organic materials decomposed by visible light.[18–20] Recently, it has been reported that the enhanced intersystem crossing rate and efficiency depend on their π-topology and linker length.[20,71] The spin polarization generated by tuning the exchange interaction and zero-field splitting in the excited states of the triplet chromophore–radical linked system has been applied to quantum technology as optical qubit initialization.[72,73] In addition, in the triplet-radical pair systems, a generation of the giant magnetization to nuclear spins in the solid matrix using the photo-induced polarization transfer has been proposed by tuning the exchange interaction and zero-field splitting of the triplet excited states of the chromophore.[74] The present study will also give useful knowledge for the structural optimization of the chromophore–radical π-conjugated systems toward applications, such as photo-DNP solid-state magic angle spinning NMR, information science, and so forth.

Conflicts of interest

There are no conflicts to declare.

Acknowledgements

This work was financially supported by the Grant-in-Aid for Scientific Research (B) (No. 20H02715) from the Japan Society for the Promotion of Science (JSPS).

Notes and references

1 Y. Teki, *Chem. – Eur. J.*, 2020, **26**, 980–996.
2 M. R. Wasielewski, M. D. E. Forbes, N. L. Frank, K. Kowalski, G. D. Scholes, J. Yuen-Zhou, M. A. Baldo, D. E. Freedman, R. H. Goldsmith, T. Goodson, 3rd, M. L. Kirk, J. K. McCusker, J. P. Ogilvie, D. A. Shultz, S. Stoll and K. B. Whaley, *Nat. Rev. Chem.*, 2020, **4**, 490–504.
3 T. Quintes, M. Mayländer and S. Richert, *Nat. Rev. Chem.*, 2023, **7**, 75–90.
4 H. Hayashi, *Introduction To Dynamic Spin Chemistry*, World Scientific Publishing Co Pte Ltd., Singapore, 2004.
5 M. L. Kirk, D. A. Shultz, J. Chen, P. Hewitt, D. Daley, S. Paudel and A. van der Est, *J. Am. Chem. Soc.*, 2021, **143**, 10519–10523.
6 M. L. Kirk, D. A. Shultz, P. Hewitt and A. van der Est, *J. Phys. Chem. Lett.*, 2022, **13**, 872–878.
7 M. L. Kirk, D. A. Shultz, P. Hewitt, J. Chen and A. van der Est, *J. Am. Chem. Soc.*, 2022, **144**, 12781–12788.
8 A. Kawai, T. Okutsu and K. Obi, *J. Phys. Chem.*, 1991, **95**, 9130–9134.
9 Y. M. Kobori, M. Masaaki, K. Akio and O. Kinichi, *Chem. Phys. Lett.*, 1996, **252**, 355–361.
10 M. T. Colvin, R. Carmieli, T. Miura, S. Richert, D. M. Gardner, A. L. Smeigh, S. M. Dyar, S. M. Conron, M. A. Ratner and M. R. Wasielewski, *J. Phys. Chem. A*, 2013, **117**, 5314–5325.
11 E. T. Chernick, R. Casillas, J. Zirzlmeier, D. M. Gardner, M. Gruber, H. Kropp, K. Meyer, M. R. Wasielewski, D. M. Guldi and R. R. Tykwinski, *J. Am. Chem. Soc.*, 2015, **137**, 857–863.
12 V. Rozenshtein, A. Berg, E. Stavitski, H. Levanon, L. Franco and C. Corvaja, *J. Phys. Chem. A*, 2005, **109**, 11144–11154.
13 D. F. Evans, *J. Chem. Soc.*, 1957, 3885–3888.
14 R. L. Ake and M. Gouterman, *Theor. Chim. Acta*, 1969, **15**, 20–42.
15 Y. Teki, S. Miyamoto, M. Nakatsuji and Y. Miura, *J. Am. Chem. Soc.*, 2001, **123**, 294–305.
16 Y. E. Kandrashkin and A. van der Est, *J. Chem. Phys.*, 2019, **151**, 184301.
17 Y. E. Kandrashkin and A. van der Est, *J. Phys. Chem. Lett.*, 2021, **12**, 7312–7318.
18 Y. Kawanaka, A. Shimizu, T. Shinada, R. Tanaka and Y. Teki, *Angew. Chem., Int. Ed.*, 2013, **52**, 6643–6647.
19 A. Shimizu, A. Ito and Y. Teki, *Chem. Commun.*, 2016, **52**, 2889–2892.
20 N. Minami, K. Yoshida, K. Maeguchi, K. Kato, A. Shimizu, G. Kashima, M. Fujiwara, C. Uragami, H. Hashimoto and Y. Teki, *Phys. Chem. Chem. Phys.*, 2022, **24**, 13514–13518.
21 Z. Wang, J. Zhao, A. Barbon, A. Toffoletti, Y. Liu, Y. An, L. Xu, A. Karatay, H. G. Yaglioglu, E. A. Yildiz and M. Hayvali, *J. Am. Chem. Soc.*, 2017, **139**, 7831–7842.
22 B. K. Rugg, M. D. Krzyaniak, B. T. Phelan, M. A. Ratner, R. M. Young and M. R. Wasielewski, *Nat. Chem.*, 2019, **11**, 981–986.
23 M. Maylander, S. Chen, E. R. Lorenzo, M. R. Wasielewski and S. Richert, *J. Am. Chem. Soc.*, 2021, **143**, 7050–7058.
24 Y. Teki, S. Miyamoto, K. Iimura, M. Nakatsuji and Y. Miura, *J. Am. Chem. Soc.*, 2000, **122**, 984–985.

25 Y. Teki, M. Nakatsuji and Y. Miura, *Mol. Phys.*, 2002, **100**, 1385–1394.
26 Y. Teki, T. Toichi and S. Nakajima, *Chem. – Eur. J.*, 2006, **12**, 2329–2336.
27 Y. Teki, S. Miyamoto and K. Koide, *Phys. Chem. Chem. Phys.*, 2015, **17**, 31646–31652.
28 M. Asano, Y. Kaizu and H. Kobayashi, *J. Chem. Phys.*, 1988, **89**, 6567–6576.
29 A. Ito, M. Hinoshita, K. Kato and Y. Teki, *Chem. Lett.*, 2016, **45**, 1324–1326.
30 I. Ciofini, P. P. Laine, M. Zamboni, C. A. Daul, V. Marvaud and C. Adamo, *Chem. – Eur. J.*, 2007, **13**, 5360–5377.
31 I. Ciofini, C. Adamo, Y. Teki, F. Tuyeras and P. P. Laine, *Chem. – Eur. J.*, 2008, **14**, 11385–11405.
32 T. Steenbock, L. L. M. Rybakowski, D. Benner, C. Herrmann and G. Bester, *J. Chem. Theory Comput.*, 2022, **18**, 4708–4718.
33 M. Franz, F. Neese and S. Richert, *Chem. Sci.*, 2022, **13**, 12358–12366.
34 F. Neese, *Wiley Interdiscip. Rev. Comput. Mol. Sci.*, 2022, **12**, e1606.
35 M. D. Hanwell, D. E. Curtis, D. C. Lonie, T. Vandermeersch, E. Zurek and G. R. Hutchison, *J. Cheminf.*, 2012, **4**, 17.
36 T. Soda, Y. Kitagawa, T. Onishi, Y. Takano, Y. Shigeta, H. Nagao, Y. Yoshioka and K. Yamaguchi, *Chem. Phys. Lett.*, 2000, **319**, 223–230.
37 D. Cho, K. Chul Ko, Y. Ikabata, K. Wakayama, T. Yoshikawa, H. Nakai and J. Y. Lee, *J. Chem. Phys.*, 2015, **142**, 024318.
38 Y. Teki, *et al.*, unpublished work.
39 Y. Teki and K. Itoh, in *Magnetic Properties of Organic Materials*, Marcel Dekker Inc., New York-Basel, 1999, pp. 237–265.
40 S. S. Kim and S. I. Weissman, *J. Magn. Reson., Ser. A*, 1976, **24**, 167–169.
41 J. Fujisawa, K. Ishii, Y. Ohba, S. Yamauchi, M. Fuhs and K. Möbius, *J. Phys. Chem. A*, 1999, **103**, 213–216.
42 J. Fujisawa, Y. Iwasaki, Y. Ohba, S. Yamauchi, N. Koga, S. Karasawa, M. Fuhs, K. Möbius and S. Weber, *Appl. Magn. Reson.*, 2001, **21**, 483–493.
43 H. Moons, E. Goovaerts, V. P. Gubskaya, I. A. Nuretdinov, C. Corvaja and L. Franco, *Phys. Chem. Chem. Phys.*, 2011, **13**, 3942–3951.
44 D. Sasikumar, A. T. John, J. Sunny and M. Hariharan, *Chem. Soc. Rev.*, 2020, **49**, 6122–6140.
45 R. Ahmed and A. K. Manna, *J. Phys. Chem. A*, 2022, **126**, 6594–6603.
46 W. T. Borden and E. R. Davidson, *J. Am. Chem. Soc.*, 1977, **99**, 4587–4594.
47 K. Itoh, T. Takui, Y. Teki and T. Kinoshita, *Mol. Cryst. Liq. Cryst.*, 1989, **176**, 49–65.
48 Y. Teki and K. Itoh, *ACS Symp. Ser.*, 1996, **644**, 16–29.
49 J. J. De Kanter, R. Kaptein and R. A. Van Santen, *Chem. Phys. Lett.*, 1977, **45**, 575–579.
50 K. Higashiguchi, K. Yumoto and K. Matsuda, *Org. Lett.*, 2010, **12**, 5284–5286.
51 M. Shinomiya, K. Higashiguchi and K. Matsuda, *J. Org. Chem.*, 2013, **78**, 9282–9290.
52 S. Nishizawa, J. Hasegawa and K. Matsuda, *Chem. Phys. Lett.*, 2013, **555**, 187–190.
53 S. Nishizawa, J. Hasegawa and K. Matsuda, *J. Phys. Chem. C*, 2013, **117**, 26280–26286.
54 S. Hasegawa and K. Matsuda, *J. Phys. Chem. C*, 2015, **119**, 5117–5121.
55 S. Hasegawa and K. Matsuda, *J. Phys. Chem. C*, 2015, **119**, 20169–20178.
56 K. Tomfohr and O. F. Sankey, *Phys. Status Solidi B*, 2002, **233**, 59–69.
57 Q. Lu, K. Liu, H. Zhang, Z. Du, X. Wang and F. Wang, *ACS Nano*, 2009, **3**, 3861–3868.
58 V. Kaliginedi, P. Moreno-Garcia, H. Valkenier, W. Hong, V. M. Garcia-Suarez, P. Buiter, J. L. Otten, J. C. Hummelen, C. J. Lambert and T. Wandlowski, *J. Am. Chem. Soc.*, 2012, **134**, 5262–5275.
59 A. M. Scott, T. Miura, A. B. Ricks, Z. E. Dance, E. M. Giacobbe, M. T. Colvin and M. R. Wasielewski, *J. Am. Chem. Soc.*, 2009, **131**, 17655–17666.
60 T. Miura, A. M. Scott and M. R. Wasielewski, *J. Phys. Chem. C*, 2010, **114**, 20370–20379.
61 A. B. Ricks, K. E. Brown, M. Wenninger, S. D. Karlen, Y. A. Berlin, D. T. Co and M. R. Wasielewski, *J. Am. Chem. Soc.*, 2012, **134**, 4581–4588.
62 T. Miura, M. Aikawa and Y. Kobori, *J. Phys. Chem. Lett.*, 2014, **5**, 30–35.
63 D. A. Shultz, R. M. Fico, H. Lee, J. W. Kampf, K. Kirschbaum, A. A. Pinkerton and P. D. Boyle, *J. Am. Chem. Soc.*, 2003, **125**, 15426–15432.
64 S. Nishizawa, J. Hasegawa and K. Matsuda, *Chem. Lett.*, 2014, **43**, 530–532.
65 C. Shu, Z. Yang and A. Rajca, *Chem. Rev.*, 2023, **123**, 11954–12003.
66 A. Bencini and D. Gatteschi, *EPR of Exchange Coupled Systems*, Springer-Verlag Berlin, Heidelberg, 1990.
67 R. McWeeny and Y. Mizuno, *Proc. R. Soc. London, Ser. A*, 1961, **259**, 554–577.
68 F. Neese, *J. Am. Chem. Soc.*, 2006, **128**(31), 10213–10222.
69 S. Sinnecker and F. Neese, *J. Phys. Chem. A*, 2006, **110**, 12267–12275.
70 K. Sugisaki, K. Toyota, K. Sato, D. Shiomi, M. Kitagawa and T. Takui, *Phys. Chem. Chem. Phys.*, 2011, **13**, 6970–6980.
71 M. Maylander, T. Quintes, M. Franz, X. Allonas, A. Vargas Jentzsch and S. Richert, *Chem. Sci.*, 2023, **14**, 5361–5368.
72 H. Mao, R. M. Young, M. D. Krzyaniak and M. R. Wasielewski, *J. Phys. Chem. B*, 2022, **126**, 10519–10527.
73 Y. Qiu, A. Equbal, C. Lin, Y. Huang, P. J. Brown, R. M. Young, M. D. Krzyaniak and M. R. Wasielewski, *Angew. Chem., Int. Ed.*, 2023, **62**, e202214668.
74 K. Kundu, T. Dubroca, V. Rane and F. Mentink-Vigier, *J. Phys. Chem. A*, 2022, **126**, 2600–2608.